Geophys. J. Int. (2008) **175,** 913–924 doi: 10.1111/j.1365-246X.2008.03948.x

Accounting for magnetic diffusion in core flow inversions from geomagnetic secular variation

Hagay Amit[1] and Ulrich R. Christensen[2]

[1]*Equipe de Géomagnétisme, Institut de Physique du Globe de Paris (Institut de Recherche associé au CNRS et à l'Université Paris 7),* 4 *Place Jussieu,* 75252 *Paris Cedex* 05, *France. E-mail: hagay@ipgp.jussieu.fr*
[2]*Max-Planck-Institut für Sonnensystemforschung,* 37191 *Katlenburg-Lindau, Germany*

Accepted 2008 August 26. Received 2008 August 22; in original form 2008 April 24

SUMMARY

We use numerical dynamos to investigate the possible role of magnetic diffusion at the top of the core. We find that the contribution of radial magnetic diffusion to the secular variation is correlated with that of tangential magnetic diffusion for a wide range of control parameters. The correlation between the two diffusive terms is interpreted in terms of the variation in the strength of poloidal flow along a columnar flow tube. The amplitude ratio of the two diffusive terms is used to estimate the probable contribution of radial magnetic diffusion to the secular variation at Earth-like conditions. We then apply a model where radial magnetic diffusion is proportional to tangential diffusion to core flow inversions of geomagnetic secular variation data. We find that including magnetic diffusion does not change dramatically the global flow but some significant local variations appear. In the non frozen-flux core flow models (termed 'diffusive'), the hemispherical dichotomy between the active Atlantic and quiet Pacific is weaker, a cyclonic vortex below North America emerges and the vortex below Asia is stronger. Our results have several important geophysical implications. First, our diffusive flow models contain some flow activity at low latitudes in the Pacific, suggesting a local balance between magnetic field advection and diffusion in that region. Second, the cyclone below North America in our diffusive flows reconciles the difference between mantle-driven thermal wind predictions and frozen-flux core flow models, and is consistent with the prominent intense magnetic flux patch below North America in geomagnetic field models. Finally, we hypothesize that magnetic diffusion near the core surface plays a larger role in the geomagnetic secular variation than usually assumed.

Key words: Inverse theory; Dynamo: theories and simulations; Geomagnetic induction; Palaeomagnetic secular variation.

1 INTRODUCTION

Since first proposed by Roberts & Scott (1965), the frozen-flux hypothesis has often been used to infer fluid motions at the top of Earth's core from geomagnetic secular variation data (Bloxham & Jackson 1991; Holme 2007). The main argument in favour of this hypothesis has been the estimate of a large value of the magnetic Reynolds number in the outer core,

$$Rm = \frac{\tau_u}{\tau_\lambda} = \frac{UL}{\lambda}, \tag{1}$$

where τ_u is magnetic advection time, τ_λ is magnetic diffusion time, U and L are typical velocity and length scales, respectively, and λ is magnetic diffusivity. Using $L = 2200\,\mathrm{km}$, $U = 5 \times 10^{-4}\,\mathrm{m\,s^{-1}}$ and $\lambda = 1\,\mathrm{m^2\,s^{-1}}$, an estimate of $Rm \sim 1000$ is obtained. This value of Rm may be misleading, for example, at the top of the core where shorter radial length scales prevail due to the presence of a hydromagnetic boundary layer, resulting in strong effects of radial diffusion (Holme 2007). Moreover, the condition $\tau_\lambda \gg \tau_u$ is not enough to justify frozen-flux; the time over which the flow evolves must be smaller than τ_λ and larger than τ_u (Braginsky & LeMouël 1993; Gubbins 1996; Gubbins & Kelly 1996). Love (1999) argued that frozen-flux fails for a nearly steady dynamo because of the coupling of steady dynamo action and secular variation and the role of magnetic diffusion in dynamo action. Bloxham (1986) argued that reversed flux patches on the core–mantle boundary are formed due to expulsion of toroidal magnetic field by radial diffusion. Several studies identified diffusive emergence and proliferation of reversed flux patches on the core–mantle boundary as a significant mechanism for the rapid decrease in the dipole intensity over the historical period (Gubbins 1987; Olson & Amit 2006). Indeed, Jackson (1997) argued that due to unmodelled diffusion effects, inverted core flows often underpredict the rate of change of the axial dipole. Tests of core-flow inversion methods using synthetic secular variation data from numerical dynamos, suggested that some inverted flow artefacts may be due to unmodelled effects of magnetic diffusion

(Rau *et al.* 2000). Including tangential magnetic diffusion (the part of magnetic diffusion that can be derived from the geomagnetic data) indeed improves the flow recovery (Amit *et al.* 2007).

Some studies proposed ways to account for the effects of magnetic diffusion on the secular variation. Voorhies (1993) suggested that advective secular variation is anticorrelated with diffusive secular variation, so, magnetic diffusion does not change the secular variation pattern but only reduces its magnitude. Gubbins (1996) developed a formalism to estimate local effects of toroidal magnetic field expulsion, by integrating the radial induction equation over patches bounded by null flux curves. Holme & Olsen (2006) estimated the relative contribution of magnetic diffusion to the secular variation based on free decay modes. They argue that although diffusion has more power at high harmonics, so does the secular variation, and the contribution of diffusion to secular variation is actually the largest at low harmonics, particularly for the dipole. They applied their magnetic diffusion estimates as uncertainties for their inverted core flow and found surprisingly little variation in the flows with respect to the flows obtained with conventional error estimates.

A different approach was taken by Olson *et al.* (2002), who inferred magnetic diffusion from numerical dynamos. They used a mean field theory to derive a balance between stretching of the large-scale magnetic field by small-scale flow and small-scale magnetic diffusion. They argued that due to the dipolarity of the field, at high-latitudes tangential magnetic diffusion is likely to be more important than radial magnetic diffusion. They demonstrated the validity of their mean field theory balance in numerical dynamos and applied their model to geomagnetic data to calculate small-scale tangential magnetic diffusion and infer small-scale core upwelling.

In this study, we also use numerical dynamos to model magnetic diffusion, but instead of relying on mean field theory we model magnetic diffusion effects based on the full terms in the induction equation. We show that the pattern of radial magnetic diffusion is correlated with the pattern of tangential magnetic diffusion for a wide range of control parameters. The relative magnitude crucially depends on the parameters. We extrapolate the amplitude ratio to Earth-like conditions and incorporate our scaled magnetic diffusion model into core flow inversions from geomagnetic secular variation data. Differences between the frozen-flux core flow models to the ones with magnetic diffusion are presented, and geophysical inferences are discussed.

2 MODEL FORMULATION

The radial component of the magnetic induction equation just below the core–mantle boundary (where radial velocity is negligible) is

$$\frac{\partial B_r}{\partial t} + \vec{u}_h \cdot \nabla B_r + B_r \nabla_h \cdot \vec{u}_h = \lambda \left[\frac{1}{R^2} \frac{\partial^2}{\partial r^2}(r^2 B_r) + \nabla_h^2 B_r \right], \quad (2)$$

where $\vec{u}_h$ is tangential velocity, r is radial coordinate, R is outer boundary radius, λ is magnetic diffusivity and $\nabla_h^2 = \nabla^2 - (1/r^2)\frac{\partial}{\partial r}(r^2 \frac{\partial}{\partial r})$. The first term on the left-hand side of (2) is the secular variation and the second and third terms represent advection of magnetic field by the flow. The first and second terms on the right-hand side represent radial and tangential magnetic diffusion, respectively.

The underlying hypothesis for inferring core flow just below the core–mantle boundary from observed geomagnetic field data is that the radial field B_r and its secular variation $\dot{B}_r$ (and consequently $\nabla_h B_r$ and $\nabla_h^2 B_r$) are practically unchanged across the very thin Ekman layer of the outer core. The Ekman layer thickness is defined by $h_{\rm ek} = h\sqrt{Ek}$ where $Ek = \nu/(\Omega h^2)$ is the Ekman number, ν kinematic viscosity, Ω the rotation rate and h the shell thickness. Monitoring the rms velocity as function of radius, we find that in fact at a depth around $h_{\rm ek}$ the transition from an increasing tangential flow magnitude inside the boundary layer to a nearly flat value below occurs. For Earth's core $Ek \sim 5 \times 10^{-15}$ (Christensen & Aubert 2006), resulting in an Ekman layer thinner than a metre when the molecular value of viscosity is used. For a turbulent viscosity similar to the magnetic diffusivity, the thickness would be of the order of hundreds of metres. In either case, the Ekman number is much larger in our models, yielding Ekman layers thicknesses of about $10^{-2}\, h$. However, both in Earth's core and in the dynamo models, in principle the same change in the role of the advection and diffusion terms in the induction equation occurs across the Ekman layer. The advective contribution to the secular variation changes dramatically across the Ekman layer, from a finite value that accounts for most of the secular variation (in nearly frozen-flux conditions) at the top of the free stream, to identically zero on the outer boundary. Another term must therefore balance the change in the advective term across the boundary layer and the only possible one is radial magnetic diffusion. Our goal is to model radial magnetic diffusion not inside the Ekman layer, but 'at the top of the free stream', the relevant depth in the context of core flow inversions.

We use 3-D self-consistent numerical dynamo models to simulate magnetic field generation by an electrically-conducting fluid flow in a rotating-convecting spherical shell. We assume fixed temperatures and rigid insulating boundaries. In most studies of numerical dynamos, either dipolar non-reversing or non-dipolar reversing dynamos were reported (Kutzner & Christensen 2002). Because we are interested primarily in modeling short-term secular variation, we restrict ourselves to dynamo models in the dipolar non-reversing regime. We use the MAGIC code (Wicht 2002).

We consider eight different models with various Rayleigh number $Ra = \alpha g_o \Delta T h^3/(\kappa\nu)$, Ekman number Ek and magnetic Prandtl number $Pm = \nu/\lambda$, where α is the thermal expansion coefficient, g_o gravity on the outer radius, ΔT the imposed temperature contrast and κ thermal diffusivity. The hydrodynamic Prandtl number $Pr = \nu/\kappa$ is fixed to one. The ratio of the Rayleigh number to the critical Rayleigh number for non-magnetic convection Ra/Ra_c is between 5 and 42. These models were chosen because they have field morphology dominated by the axial dipole, the most geophysically relevant case, and the non-dipole part of the field shows some resemblance to the geomagnetic field, for example, in the existence of high-latitude flux lobes. Reversed flux patches can be seen emerging, growing and intensifying on the outer boundary of the simulations, as observed in the present geomagnetic field. These magnetic structures are associated with diffusive processes and their growth and intensification contribute to the decrease in the models' dipole intensity (Olson & Amit 2006), as was suggested for Earth's modern field (Gubbins 1987). The magnetic Reynolds number Rm covers a range from 100 to 1000 in our various model cases. Christensen & Tilgner (2004) showed that the characteristic timescale of secular variation depends on the inverse of the magnetic Reynolds number, and that models with $Rm \approx 1000$ have the same secular variation time as the present geomagnetic field, when time is scaled with the magnetic diffusion time in the model. However, although overall the timescale of secular variation in the model matches that in the geomagnetic field, specific contributions to the secular variation arising from oscillatory motions may differ. In the model, the characteristic timescales for advection, inertial waves and torsional oscillations are rather similar, whereas in the Earth's core they differ more strongly.

Each model has been run until a statistical equilibrium was reached. Then 10 snapshots at different times are taken, for which radial and tangential diffusion terms on the right-hand side of (2) at various depths are computed. We concentrate in particular on their values at the top of the free stream, at a depth of $h_{\rm ek}$ below the outer boundary. For each of the model snapshots, we compute the correlation coefficient C and the rms ratio of the two diffusion terms D,

$$C = \frac{\int_S \left[\frac{1}{r^2}\frac{\partial^2}{\partial r^2}(r^2 B_r)\right] \nabla_h^2 B_r \, \mathrm{d}S}{\sqrt{\int_S \left[\frac{1}{r^2}\frac{\partial^2}{\partial r^2}(r^2 B_r)\right]^2 \mathrm{d}S}\sqrt{\int_S \left(\nabla_h^2 B_r\right)^2 \mathrm{d}S}}, \tag{3}$$

$$D = \sqrt{\frac{\int_S \left[\frac{1}{r^2}\frac{\partial^2}{\partial r^2}(r^2 B_r)\right]^2 \mathrm{d}S}{\int_S \left(\nabla_h^2 B_r\right)^2 \mathrm{d}S}}, \tag{4}$$

where $\mathrm{d}S = r^2 \sin\theta \mathrm{d}\theta \mathrm{d}\phi$ is a spherical surface increment and S is the spherical surface. We analyse the dependence of the ratio D on the various control parameters. We also calculated the relative magnitude of radial diffusion with respect to the total secular variation:

$$R = \sqrt{\frac{\int_S \left[\lambda \frac{1}{r^2}\frac{\partial^2}{\partial r^2}(r^2 B_r)\right]^2 \mathrm{d}S}{\int_S (\partial B_r/\partial t)^2 \, \mathrm{d}S}} \tag{5}$$

and similarly that of tangential diffusion

$$H = \sqrt{\frac{\int_S \left(\lambda \nabla_h^2 B_r\right)^2 \mathrm{d}S}{\int_S (\partial B_r/\partial t)^2 \, \mathrm{d}S}}. \tag{6}$$

We first determine these statistical measures using the magnetic field at the full resolution of the model, which varies depending on parameters between 64 and 133 for the maximum harmonic degree and order. Because only the long wavelength part of the geomagnetic field at the core–mantle boundary is known, we also calculated the correlation coefficient and amplitude ratio between radial and tangential diffusion for a lowpass filtered magnetic field. The filter passes all spherical harmonic degrees until $l = 12$ unchanged and suppresses all degrees $l > 14$ with a cosine tapering function in between, resulting in a similar spatial resolution for the magnetic field as in core field models (e.g. *gufm1* of Jackson *et al.* 2000). We use the suffix 'f' to denote statistical properties obtained for the filtered fields.

The 95 per cent confidence level for the statistical significance of a correlation between two fields with F degrees of freedom is approximately given by a value of $C_c = 1.97/\sqrt{F}$ for the correlation coefficient (Press *et al.* 1989). For a field resolved up to a spherical harmonic degree of 12, $F = 168$, and we get $C_c \simeq 0.15$. This value will be used as a threshold for determining statistically significant correlations.

3 RESULTS

3.1 Correlation coefficients and amplitude ratios

In case 1, with a high value of the Ekman number and a moderate Rayleigh number that is approximately five times larger than that for the onset of convection, the magnetic field structure is dominated by large scales. A fair degree of correlation of the spatial pattern of radial and tangential diffusion is obvious (Fig. 1). The correlation coefficient is $C = 0.56$ at the top of the free stream, averaging the results for ten arbitrary snapshots (Table 1). This

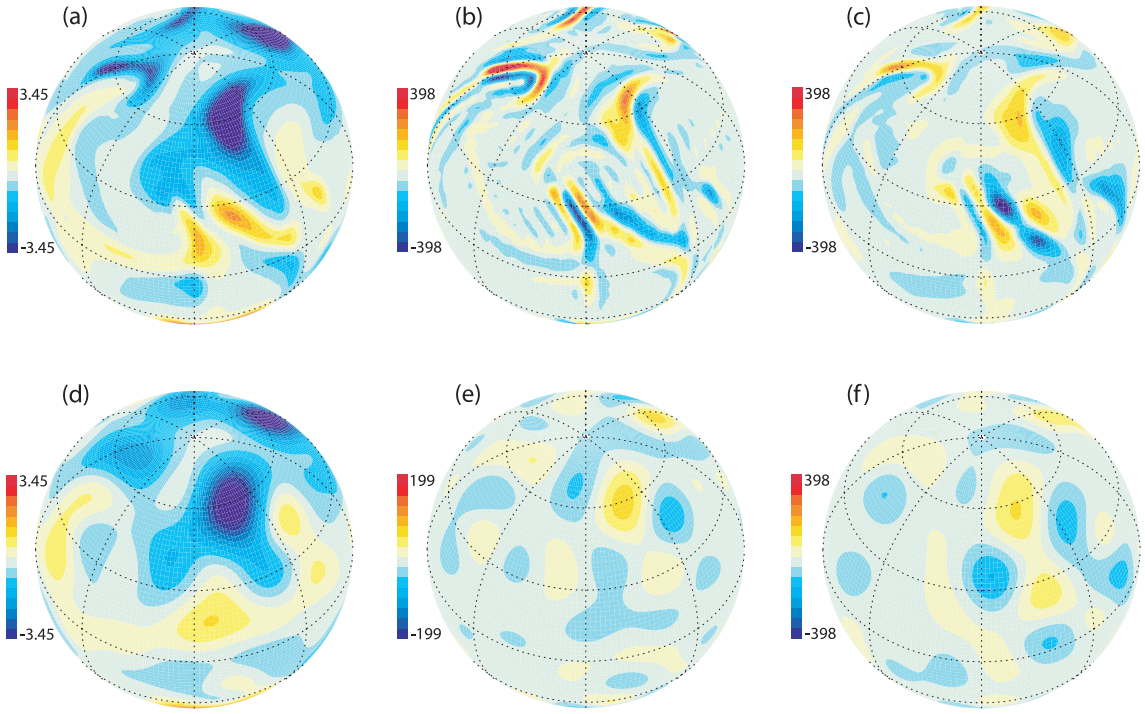

Figure 1. Radial magnetic field (a), tangential magnetic diffusion (b) and radial magnetic diffusion (c) for a snapshot of case 1. The corresponding quantities for a lowpass filtered field are given in (d)–(f), respectively. All images are at the top of the free stream. Red stands for positive values and blue for negative. Note that the filtered tangential magnetic diffusion term is enhanced by a factor of two with respect to the other diffusion terms. In this snapshot $C = 0.52$, $D = 0.88$, $C_f = 0.61$ and $D_f = 2.11$.

Table 1. Correlation coefficient C, constant of proportionality D and the rms ratios between radial diffusion and secular variation R and between tangential diffusion and secular variation H.

Case	Ra	Ra/Ra_c	Ek	Pm	Rm	C	D	R	H	C_f	D_f	R_f	H_f
1	$3 \cdot 10^5$	5.37	10^{-3}	4	112	0.56	0.78	0.42	0.54	0.56	2.30	0.53	0.23
2	$1.5 \cdot 10^6$	7.39	$3 \cdot 10^{-4}$	2	96	0.52	1.37	0.78	0.57	0.37	4.08	1.02	0.25
3	$3 \cdot 10^6$	14.78	$3 \cdot 10^{-4}$	3	296	0.60	1.19	0.32	0.27	0.38	5.30	0.53	0.10
4	$8 \cdot 10^6$	25.00	$2 \cdot 10^{-4}$	3	487	0.61	1.69	0.27	0.16	0.38	8.17	0.49	0.06
5	$1.5 \cdot 10^7$	21.52	10^{-4}	2	330	0.64	1.68	0.37	0.22	0.32	7.56	0.68	0.09
6	$8 \cdot 10^6$	11.48	10^{-4}	2	177	0.57	1.64	0.59	0.36	0.30	5.75	0.92	0.16
7	$1.5 \cdot 10^7$	21.52	10^{-4}	4	617	0.63	1.92	0.25	0.13	0.35	7.33	0.44	0.06
8	$1.2 \cdot 10^8$	42.40	$3 \cdot 10^{-5}$	2.5	925	0.66	1.61	0.29	0.18	0.24	10.00	0.50	0.05

Note: All values are at depth h_{ek} obtained by weighted average of values from neighbouring radial grid levels and averaged over ten arbitrary snapshots. The suffix 'f' denotes values for lowpass filter fields. Case 8 is from Christensen & Aubert (2006), the other cases are from this study.

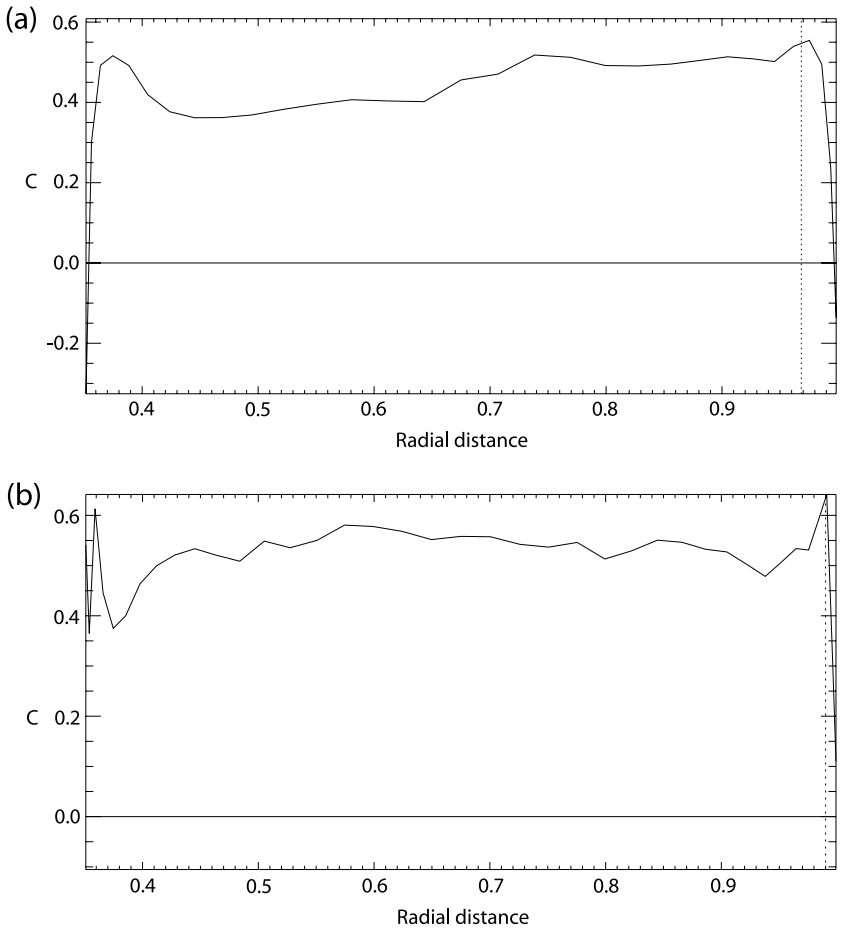

Figure 2. Correlation coefficients between radial and tangential magnetic diffusion as a function of depth (in units of shell thickness) for snapshots of cases 1(a) and 7(b). Dotted vertical lines indicate the top of the free stream (depth h_{ek}).

value of C is very significant, given the many degrees of freedom (order 1000) in the two fields. Deeper in the shell the correlation degrades slightly, reaching $C = 0.45$ at mid-depth (Fig. 2) in this case. The relative magnitudes of the two diffusive contributions vary more significantly with depth. At the top of the free stream the amplitude ratio of radial to tangential magnetic diffusion is $D = 0.78$, whereas at the centre of the shell the ratio drops to 0.26. The standard deviations of C and D for different snapshots in this case as well as in other cases are rather low, usually less than 10 per cent.

The correlation holds surprisingly well and even better for dynamos in which the magnetic field is dominated by smaller scales. For example, in case 7, with an Ekman number of 10^{-4} and a Rayleigh number that is 22 times supercritical, the correlation at the top of the free stream is $C = 0.63$, and the amplitude ratio is $D = 1.92$ (Table 1). At the centre of the shell, the correlation slightly degrades to 0.56 (Fig. 2) and D drops to 0.30. Table 1 summarizes the correlation coefficients and amplitude ratios of the two diffusive terms at depth h_{ek} for different dynamo simulations. The correlation coefficient does not vary by much, but in general improves slightly with decreasing values of the Ekman number and increasing values for the Rayleigh number. The correlation holds everywhere in the shell with best correlations near the edge of the Ekman boundary layer.

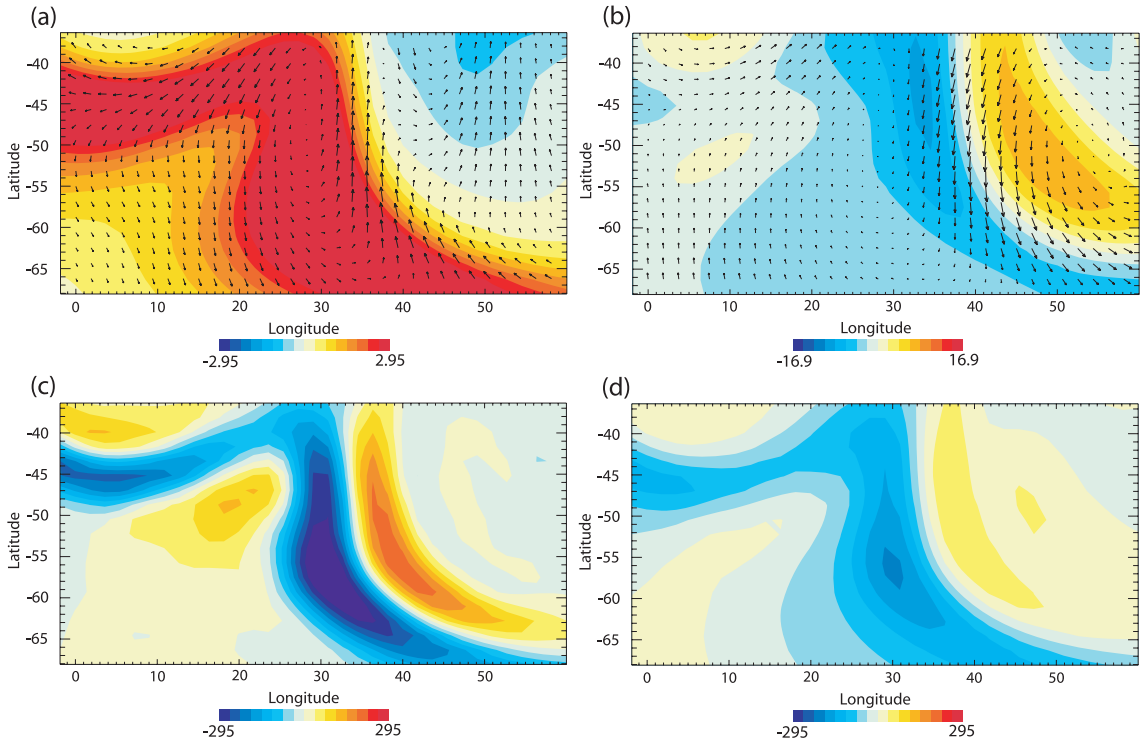

Figure 3. Close-up of a region of interest at high southern latitudes of Fig. 1. Radial (colors) and tangential (arrows) magnetic field (a), radial and tangential velocity (b), tangential magnetic diffusion (c) and radial magnetic diffusion (d).

We find that diffusion contributes not dominantly, but significantly to the secular variation, that is, the ratios R and H range between 0.1 and 0.8 (Table 1). As expected, the ratio of tangential diffusion to secular variation decreases with filtering, that is, $H_f < H$, because the long scales do not diffuse efficiently. In contrast, the ratio of radial diffusion to secular variation increases slightly with filtering $R_f > R$. Toward lower Ekman numbers and higher Rayleigh numbers convection is more vigorous and exhibits more small-scale features, and the two tendencies generally sharpen, that is, $H_f \ll H$ and $R_f \gg R$. H_f becomes much smaller than one, whereas R_f remains of the order of one, with no clear trend when the Ekman and Rayleigh numbers are changed. It is therefore expected that at Earth-like conditions, radial diffusion will play a significant role for the large-scale truncated geomagnetic field at the core–mantle boundary.

3.2 Physical mechanisms

To shed light on the physical causes for the correlation between radial and tangential diffusion, we focus on two regions of case 1, whose global pattern is shown in Fig. 1. Fig. 3 focuses on a high-latitude region with intense normal flux, and Fig. 4 focuses on a mid-latitude region where an inverse flux spot appears. Tangential magnetic diffusion is related in a simple way to the spatial distribution of magnetic flux $B_r(\phi, \theta)$. It acts to disperse B_r horizontally. Therefore, ridges of intense B_r patches anticorrelate with tangential magnetic diffusion, whereas at the margins of these structures tangential magnetic diffusion acts to strengthen B_r. For the Earth's magnetic field $\partial B_r/\partial r$ and hence radial magnetic diffusion is unknown. However, note the remarkable anticorrelation between radial magnetic diffusion and B_r. Intense B_r structures are associated with downwelling at the top of the core (Christensen *et al.* 1998; Olson & Christensen 2002). Radial diffusion expels magnetic flux through the centres of the convective columns (Gubbins *et al.* 2000) as is suggested by local energy balance at each column (Olson *et al.* 1999). Therefore, radial and tangential magnetic diffusion terms share similar locations for the centres of their main structures. Discrepancies appear at the margins of flux concentrations where tangential magnetic diffusion strengthens B_r whereas radial magnetic diffusion still weakens B_r. Overall, tangential magnetic diffusion is characterized by smaller length scales whereas radial magnetic diffusion has a similar length scale as B_r.

In Fig. 5, we show a similar close-up image taken at a greater depth of $4.6h_{\rm ek}$. The pattern agreement here, and in general in the shell (Fig. 2), indicates that the correlation of the two diffusion terms is more than just a boundary layer effect. However, the amplitude ratio of radial and tangential magnetic diffusion is smaller at depth. In a columnar vortex, radial flow is stronger in the interior, so, $\partial B_r/\partial r$ is weaker in the interior, and therefore radial diffusion is also weaker there.

The correlation also holds for dynamos whose magnetic field is dominated by smaller scales. We show global maps at the top of the free stream for case 7 (Fig. 6). At full resolution the small length scales make it difficult to get a visual impression of the correlation, but the correlation coefficient is actually slightly higher than in the case with higher Ekman number and lower Rayleigh number (see Table 1). The correlation is more obvious upon visual inspection for the low-pass filtered fields.

The physical mechanism for the correlation of the two diffusive terms is schematically illustrated in Fig. 7. As an example, we consider a cyclonic columnar vortex parallel to the rotation axis that intercepts the core–mantle boundary at mid-to-high latitudes in both hemispheres. The existence of such columnar flow structures in the core has been inferred from the high-latitude flux lobes in the geomagnetic core field (Gubbins & Bloxham 1987) and is supported by theoretical studies of fast rotating convective systems

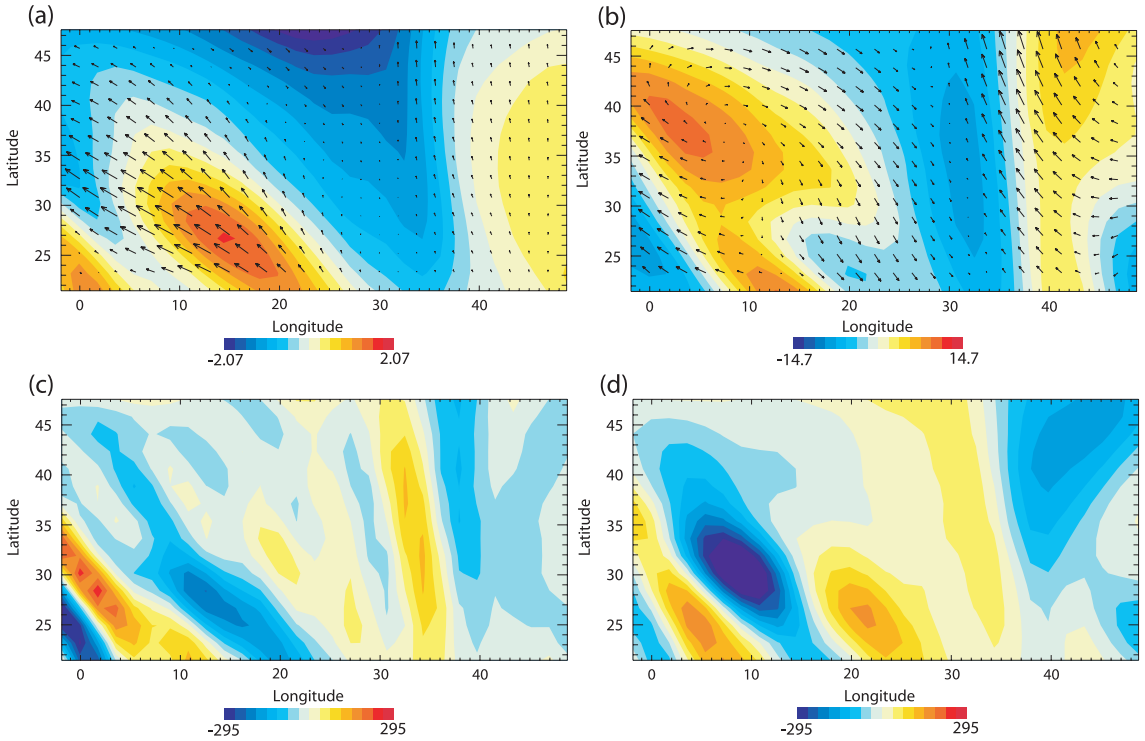

Figure 4. As in Fig. 3 in a region at northern mid-latitudes of Fig. 1.

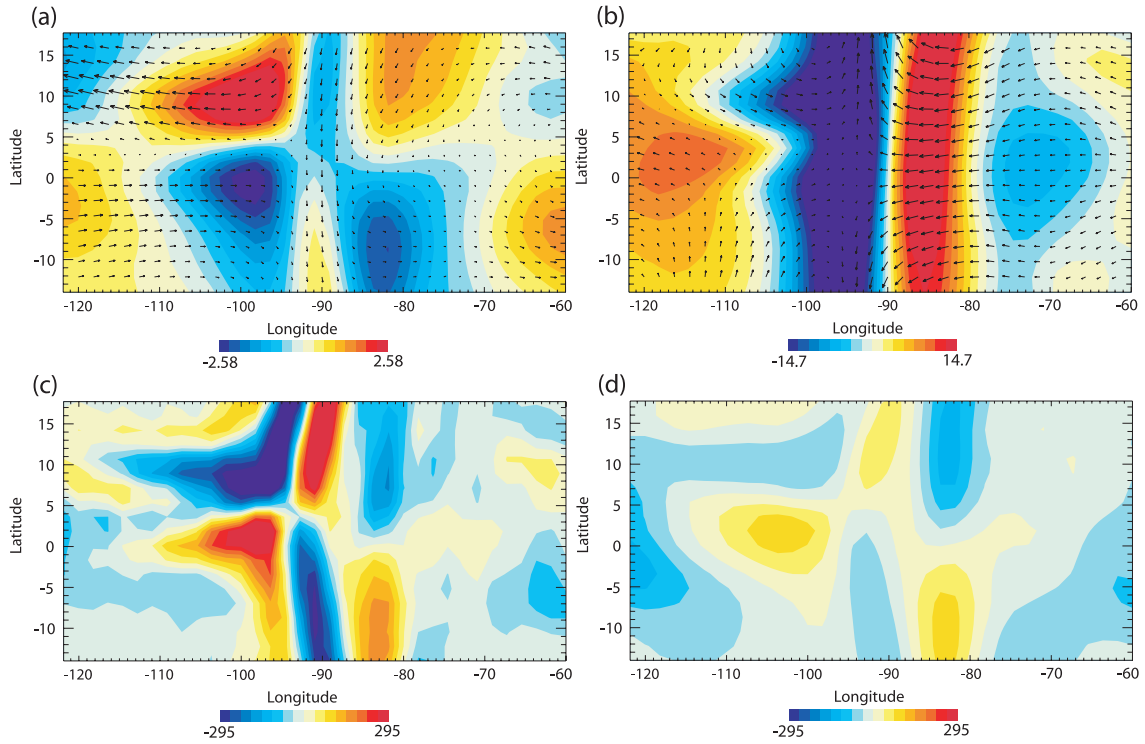

Figure 5. Close-up for an area at a depth of $4.6h_{\rm ek}$ in case 1. The global correlation coefficient and amplitude ratio at this level have values of $C = 0.51$, $D = 0.33$, $C_f = 0.55$ and $D_f = 0.72$.

(Busse 1975), self-consistent numerical dynamos (Olson *et al.* 1999; Aubert *et al.* 2008) and was recently used as a constraint in core flow inversions (Pais & Jault 2008). Cyclonic vortices are associated with surface downwelling (Olson *et al.* 2002; Amit & Olson 2004). The descending flow is accompanied by surface convergence that concentrates intense radial magnetic field (positive B_r in our example). Tangential magnetic diffusion acts to smear B_r horizontally. At depth convergence is weaker, and the radial field becomes less concentrated by the flow. Therefore, $\partial B_r/\partial r$ is positive and magnetic flux diffuses inward at the centre of the convective column,

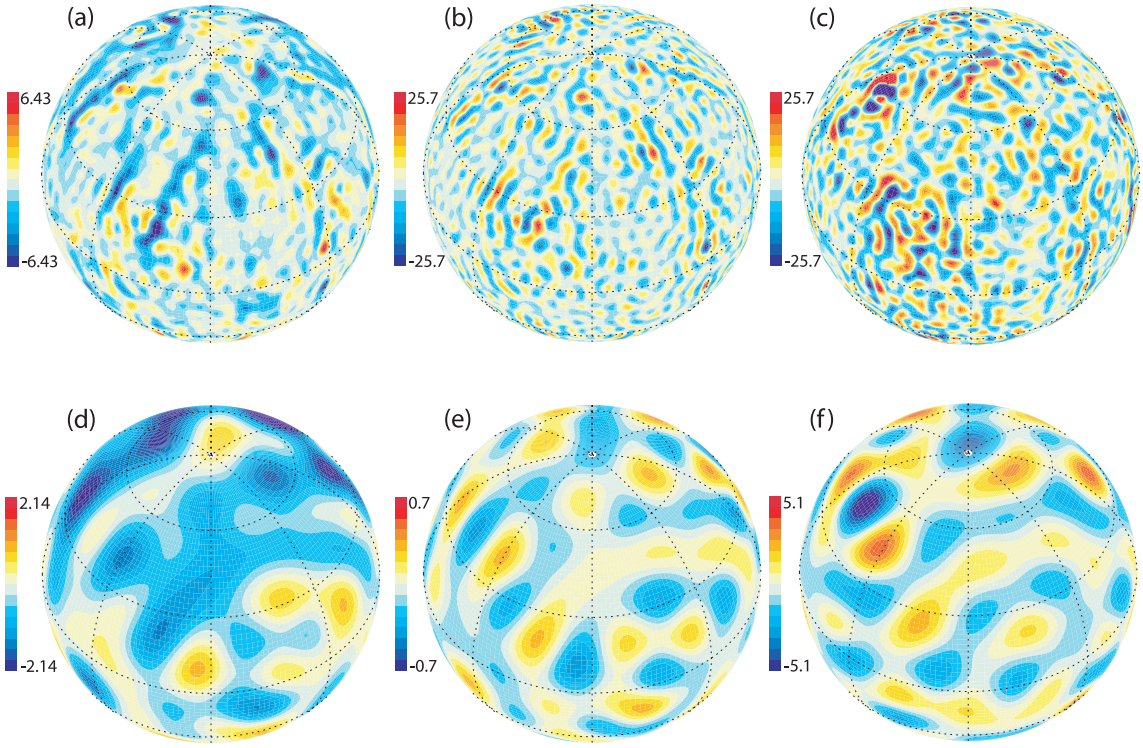

Figure 6. Same as Fig. 1 for dynamo case 7 at the top of the free stream. Note that the contour interval for the filtered B_r is smaller by a factor of three compared with that for the unfiltered, the filtered tangential diffusion is enhanced by a factor of 35 and the filtered radial diffusion is enhanced by a factor of five. In this snapshot, $C = 0.59$, $D = 1.48$, $C_f = 0.48$ and $D_f = 6.72$.

acting to weaken the surface B_r. The result is a correlation between negative structures of radial and tangential magnetic diffusion that are associated with an intense positive B_r structure on the outer boundary.

We note that the positive ratio between radial and tangential diffusion terms does not hold universally. In particular, at the centre of a growing flux spot that emerges diffusively through the core surface, the relation between radial and tangential diffusion changes sign. We find that the positive correlation is restored, once the flux patch is mature (e.g. Fig. 4).

3.3 Data truncation effects

Geomagnetic core field models are typically truncated at spherical harmonic degree 14 due to the dominance of the crustal magnetic field at higher degrees. It is therefore important to examine the scale dependence of the correlation between radial and tangential magnetic diffusion. In dynamo case 1, the magnetic field and the two diffusion fields are fairly large-scale, even without filtering (Fig. 1). The spatial correlation C_f between filtered radial diffusion and filtered tangential diffusion is adequate, and in the specific snapshot shown in Fig. 1, even better than in the non-filtered case. In general, the non-filtered and filtered correlations are comparable in this case (Table 1). However, the factor of proportionality D_f is significantly different from its non-filtered value. Tangential magnetic diffusion is characterized by smaller scales than radial diffusion, so filtering results in a significantly larger value of D_f (note the factor 2 enhancement for the filtered tangential diffusion term in Fig. 1).

In case 7, which contains substantial energy at small spatial scales, the correlation coefficient decreases for the filtered fields, although the agreement in pattern of the two diffusion terms is still decent in the snapshot shown in Fig. 6. Also note that in this case, radial diffusion at the top of the free stream is about seven times more intense than tangential diffusion at large wavelengths. For the total (unfiltered) fields, the ratio is about two.

Considering the time-averages of 10 arbitrary snapshots for all our dynamo models (Table 1), we find that, except for the dynamo case 1 that is intrinsically large-scaled, the correlation degrades upon lowpass filtering. However, despite decreasing values of the correlation coefficients C_f in smaller-scale dynamos, the coefficients are still well above the level of statistical significance C_c. The amplitude ratios D and D_f generally increase on approach to more Earth-like parameter values, but the ratio D_f for the filtered field does so more strongly.

4 EXTRAPOLATION TO THE EARTH

We propose to approximate the full magnetic diffusion term at the top of the free stream in the Earth's outer core by scaling up the tangential diffusion according to

$$\lambda \frac{1}{r} \nabla^2 (r B_r) \simeq \lambda (D+1) \nabla_h^2 B_r. \qquad (7)$$

We must estimate the value of the numerical constant D for Earth-like conditions. D seems to be scale-dependent and for practical applications, we are mostly interested in its value for the large-scale magnetic field D_f. Our analysis of the dynamo models suggests that D and D_f increase as the Ekman number decreases and the Rayleigh number increases.

We attempted a general power-law fit for D as a function of all three control parameters *Ra*, *Ek* and *Pm*. We found that the influence of *Pm* is weak, and we obtained similar exponents for *Ra* and *Ek*, with that for Ekman number being slightly larger. This suggested

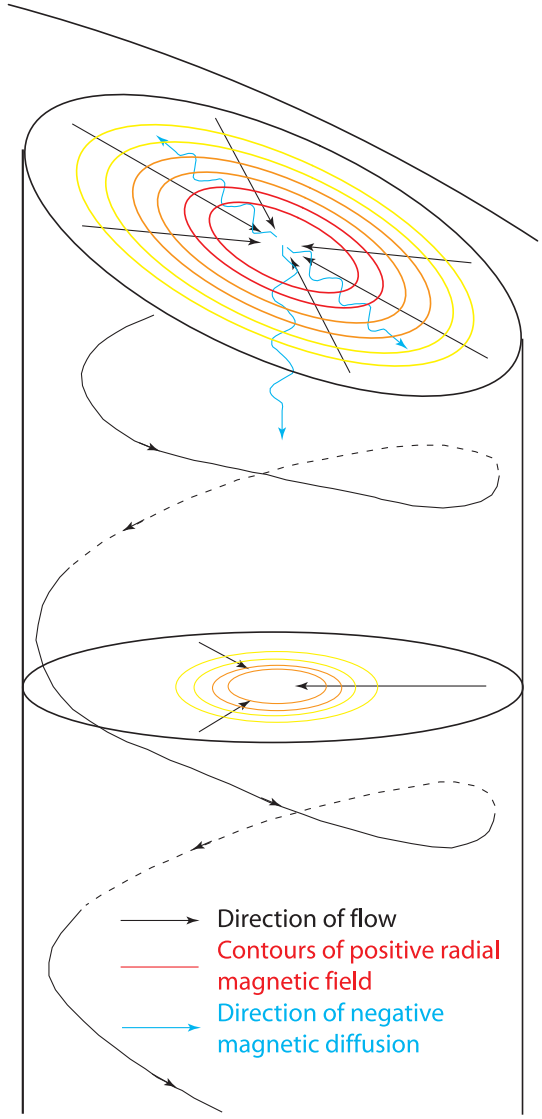

Figure 7. Schematic illustration of the physical mechanism responsible for the correlation between radial and tangential magnetic diffusion.

to us that D and D_f depend primarily on the Rayleigh number normalized by its critical value Ra_c. At very small values of the Ekman number, this ratio varies as $RaEk^{4/3}$.

In Fig. 8, we plotted the mean values of D and D_f from our models versus Ra/Ra_c. A linear regression analysis provides for D the relation

$$D = 0.62(Ra/Ra_c)^{0.31}. \tag{8}$$

For D_f the fit is better and the exponent and prefactor are larger:

$$D_f = 0.95(Ra/Ra_c)^{0.66}. \tag{9}$$

The absolute scatter in the D and D_f fits is similar, but the D_f correlation is better due to the steeper slope. With increasing vigour of the flow at more strongly supercritical values of the Rayleigh numbers, the spatial scale of the magnetic field becomes smaller in the horizontal direction. In the radial direction, it seems to shrink even more strongly near the outer boundary, where a magnetic boundary layer is formed. Hence the ratio D between radial and tangential diffusion increases with Ra/Ra_c. Because the reduction in horizontal scale is not relevant for the low-pass filtered field, but the radial scale should be affected in a similar way for smaller and larger horizontal wavelengths, the dependence of D_f on the Rayleigh number is more pronounced than it is for D.

The value of the Rayleigh number in the Earth's core is not well constrained. Based on a scaling law for the flow velocity and on a characteristic value for the flow at the top of the Earth's core deduced from secular variation, Christensen & Aubert (2006) estimated the normalized Rayleigh number to be 5000. Using this value in our fitting laws, we obtain for the Earth's core $D \approx 8.5$ and $D_f \approx 260$.

The magnetic diffusivity λ of the outer core is primarily estimated from mineral physics experiments and theoretical extrapolations (for review see Poirier 2000). At the top of the core its value is likely in the range of $1–3\,\mathrm{m^2\,s^{-1}}$ (Secco & Schloessin 1989; Stacey & Loper 2007). To account for radial diffusion at the top of the core, we define an effective magnetic diffusivity acting on the horizontal Laplacian of B_r in (7) as

$$\lambda^* = \lambda(D + 1). \tag{10}$$

For the observable large-scale magnetic field relevant for core flow inversions, the good fit for D_f as function of normalized Rayleigh number suggests that values of the order of $10^2–10^3\,\mathrm{m^2\,s^{-1}}$ are appropriate for λ^*.

5 CORE FLOW INVERSIONS WITH MAGNETIC DIFFUSION

We have used geomagnetic core field models of $B_r(\phi, \theta)$ for calculating $\nabla_h^2 B_r$, and we inverted the observed geomagnetic secular variation for the flow at the top of the core, taken horizontal magnetic diffusion and, in parametrized form, radial magnetic diffusion into account. More specifically, we invert the following equation:

$$\frac{\partial B_r}{\partial t} + \vec{u}_h \cdot \nabla B_r + B_r \nabla_h \cdot \vec{u}_h = \lambda^* \nabla_h^2 B_r. \tag{11}$$

We employed the inversion method of Amit & Olson (2004, 2006), with the helical flow assumption. Here the formal non-uniqueness that is inherent to core flow inversions is removed by assuming a linear relation between the tangential flow divergence and the radial vorticity ζ at the top of the free stream

$$\nabla_h \cdot \vec{u}_h = \mp k\zeta, \tag{12}$$

where the minus sign applies in the Northern Hemisphere and the plus sign in the Southern Hemisphere. We set $k = 0.15$ and we do not include a tangential geostrophy constraint on the flow. This specific k value was found to optimize the fit to the length of day variation inferred from the core flow models (Amit & Olson 2006). As described in Amit & Olson (2004), $\vec{u}_h$ is expressed by toroidal and poloidal potentials for which a set of advection–diffusion equations can be derived from (11) and (12). These are solved on a spatial grid of $5^\circ \times 5^\circ$ degrees at the core surface. We note that unlike in the classical methods of core flow inversions, which do not make the helical flow assumption and use a spherical harmonic expansion of the flow field, our method does not require an additional regularization (smoothness) condition. We inverted for single epoch flows between 1840–1990 in 5 yr intervals, based on the geomagnetic secular variation model of Jackson *et al.* (2000). Various calculations were performed: one assuming frozen-flux (i.e. $\lambda^* = 0$) and several with magnetic diffusion based on (7), where we increase the effective magnetic diffusivity stepwise up to $\lambda^* = 400\,\mathrm{m^2\,s^{-1}}$.

We find that the diffusive solutions differ only marginally from the frozen-flux solutions for $\lambda^* < 100\,\mathrm{m^2\,s^{-1}}$. At $\lambda^* = 200\,\mathrm{m^2\,s^{-1}}$, the differences become appreciable, and at $\lambda^* = 400\,\mathrm{m^2\,s^{-1}}$, they

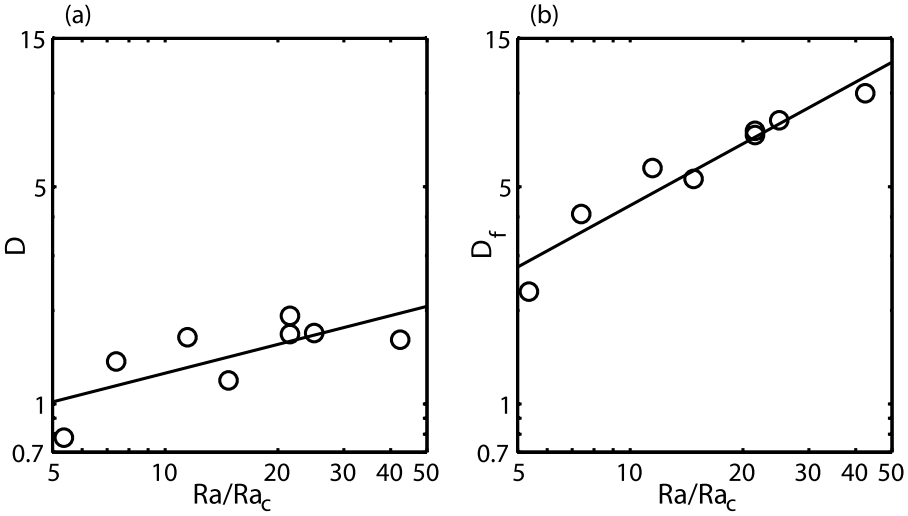

Figure 8. Power-law fits for D (a) and D_f (b) as function of Ra/Ra_c.

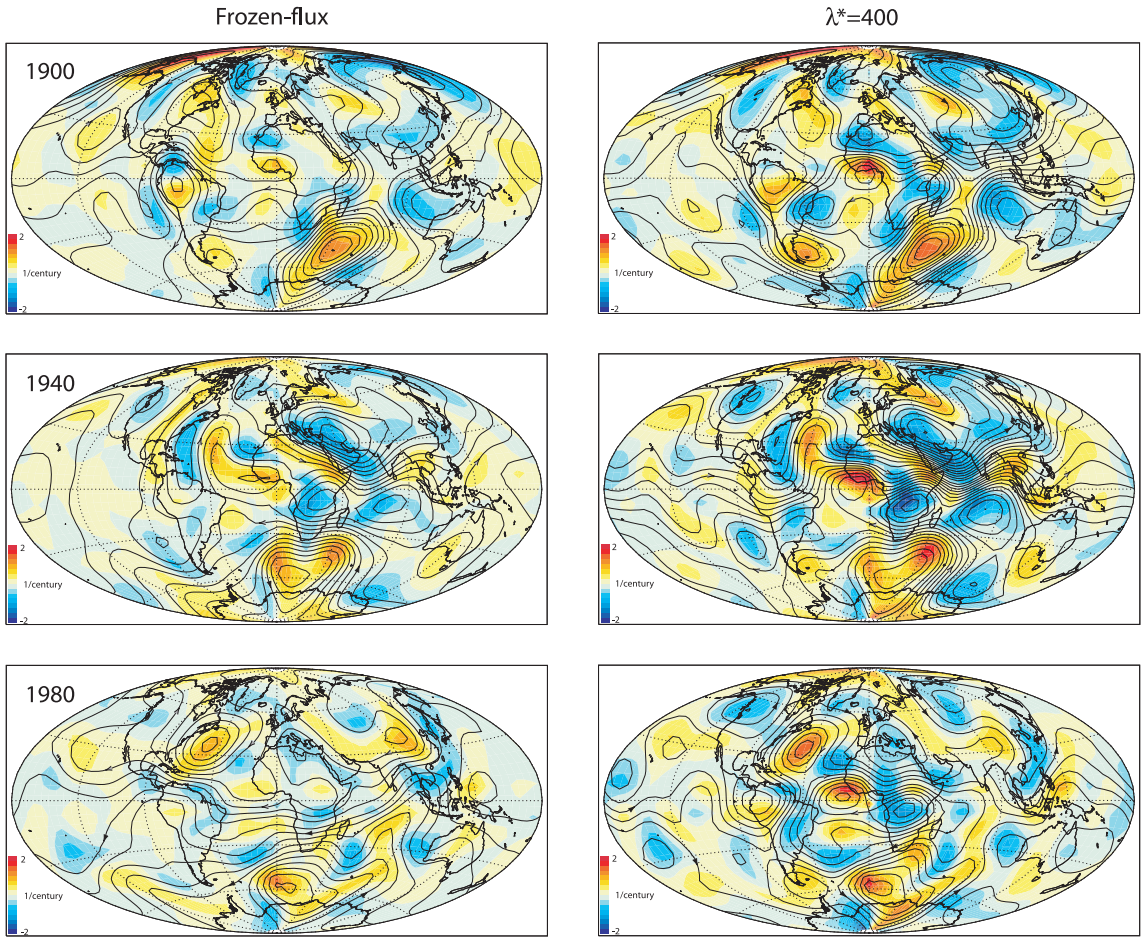

Figure 9. Inverted core flow models: frozen-flux (left-hand column), and with effective magnetic diffusivity $\lambda^* = 400\,\mathrm{m^2\,s^{-1}}$ (right-hand column), for 1900 (top row), 1940 (middle) and 1980 (bottom row). Contours are streamlines (contour intervals are the same for all plots), with arrows indicating the direction of circulation. Red/blue background colors indicate upwelling/downwelling, respectively.

are fairly pronounced in some regions of the core surface. The rms velocities are of the order of 10 km yr^{-1} in the frozen-flux solutions. They are slightly larger at $\lambda^* = 200\,\mathrm{m^2\,s^{-1}}$ and approximately 30–50 per cent larger at $\lambda^* = 400\,\mathrm{m^2\,s^{-1}}$. In Fig. 9, we compare the frozen-flux solutions with those obtained with $\lambda^* = 400\,\mathrm{m^2\,s^{-1}}$ for 1900, 1940 and 1980. These years have been arbitrarily chosen, avoiding the edges in time of the geomagnetic field model.

Prominent large-scale flow structures in our frozen-flux core flow snapshots (left-hand column of Fig. 9) include a large anticlockwise vortex in the Southern Hemisphere below the Indian and Atlantic

Oceans, a clockwise vortex below North America, an anticlockwise vortex below Asia and a westward flow in the mid- and low-latitudes of the Atlantic Southern Hemisphere (Amit & Olson 2006). These large-scale flow features are common to other core flow models derived using different physical assumptions and inversion methods (Bloxham 1989; Jackson *et al.* 1993; Chulliat & Hulot 2000; Holme & Whaler 2001; Hulot *et al.* 2002; Eymin & Hulot 2005; Holme 2007; Pais & Jault 2008).

The global impact of including magnetic diffusion is moderate. The same large-scale flow features that appear in the frozen-flux flows (left column of Fig. 9) can still be identified in the diffusive flows (right columns of Fig. 9) in a given snapshot. However, a detailed examination reveals significant local effects that magnetic diffusion may have on the inferred core flow. We note four regions where including magnetic diffusion results in pronounced differences in the inverted core flow morphology: (1) At low-latitudes in the Pacific, where the flow is weak and generally westward in the frozen-flux solutions, it turns into an eastward flow in the diffusive case, (2) eastward flow appears below the Atlantic and Africa north of the equator, which is not present in the frozen-flux case except in the solution for 1940, (3) with diffusion, the clockwise vortex below North America weakens for 1900 and an anticlockwise vortex emerges in 1940 and 1980 and (4) the Asian anticlockwise vortex strengthens in the solution for 1900 and 1980.

Fig. 9 also shows the upwelling pattern representing the poloidal component of the flow. Poloidal flow is tightly linked to diffusion effects by magnetic flux expulsion processes (Bloxham 1986; Gubbins 1996). In our inversions, toroidal and poloidal flows are coupled by the helical flow assumption, so that the overall intensification of the flow affects both components equally.

6 GEOPHYSICAL IMPLICATIONS

Our results have several important geophysical implications, including: (1) the Atlantic/Pacific secular variation dichotomy, (2) long-term thermal core–mantle coupling, and (3) the validity of the frozen-flux approximation on short timescales. Here we discuss these geophysical implications and compare our findings with those of previous studies.

The Pacific region is characterized by low geomagnetic secular variation in modern satellite data (Hulot *et al.* 2002), throughout the past 400 yr (Jackson *et al.* 2000), and even in the palaeomagnetic record (Gubbins & Gibbons 2004). In frozen-flux core flow models this results in a clear dichotomy between the active Atlantic and quiet Pacific hemispheres (Hulot *et al.* 2002; Amit & Olson 2006). Christensen & Olson (2003) and Gubbins & Gibbons (2004) hypothesized that the low Pacific secular variation is related to low heat flux extracted from the core–mantle boundary in that region (as suggested by low seismic shear velocity in the lowermost mantle), which suppresses core convection there. Including magnetic diffusion indicates that the Pacific hemisphere may be more active than in the frozen-flux models, although flow in the Atlantic hemisphere is still more vigorous. It may seem counter-intuitive to expect significant flow in regions of low secular variation, but physically plausible examples for dynamos have been given where advection and diffusion cancel to give no secular variation despite strong flow (Love 1999). However, the possibility for cancellation is no positive proof for flow in the Pacific and we note that the predicted flow patterns at low latitudes, where most of the changes occur in the Pacific, are probably less robust than they are at mid and high latitudes. At low latitudes the helical flow assumption is probably less justified and at the equator, it breaks down entirely, which is expressed by the abrupt change in sign in (12).

A recent study by Aubert *et al.* (2008) explains several geophysical observations of non-axisymmetric core dynamics and properties using a numerical dynamo with heterogeneous outer boundary heat flux inferred from a lower mantle seismic shear velocity model (Masters *et al.* 2000). One region where the flow comparison fails is below North America, where several core flow models find a clockwise vortex (Amit & Olson 2006; Pais & Jault 2008), but the model of Aubert *et al.* (2008), as well as a simple mantle-driven thermal wind prediction (Amit *et al.* 2008) require an anticlockwise vortex. Moreover, to maintain the prominent intense magnetic flux patch below North America, convergence is necessary, and therefore a cyclone is expected. In our diffusive core flow models, indeed a cyclone emerges below North America. Also, the Asian cyclone that Aubert *et al.* (2008) found crucial for explaining the inner-core east–west hemispherical dichotomy in seismic velocity is strengthened in our diffusive core flow models.

The increasing magnitude of the inverted core flow velocity, both toroidal and poloidal, with increasing effective magnetic diffusivity suggests that in some regions below the core–mantle boundary magnetic advection and diffusion are nearly in balance, and the secular variation is a small residual, as was previously proposed (Gubbins & Kelly 1996; Love 1999). This seems to be the case at low latitudes below the Pacific and northern equatorial Africa. As a result, frozen-flux flow models cannot depict flow structures in these regions, where our diffusive models suggest that some flow activity exists. However, in most regions, similar flow structures that appear in the frozen-flux flows can be identified in the diffusive flows, which in general supports the usefullness of the frozen-flux approximation.

7 DISCUSSION AND CONCLUSIONS

In numerical dynamo simulations, we have found that radial magnetic diffusion at the top of the free stream is positively correlated with tangential diffusion. We suggest parameterizing radial diffusion, which cannot be determined from geomagnetic field models, in terms of the 'observable' tangential diffusion for the purpose of inverting geomagnetic secular variation for the flow near the core surface. At the large resolvable scales of the core magnetic field, tangential diffusion contributes very little to the secular variation. However, we find in the dynamo models that the effect of radial diffusion on the large-scale field becomes significantly stronger than that of tangential diffusion, in particular when we vary the model parameters in the direction of more Earth-like values.

Parameterizing radial diffusion by a strongly enhanced diffusivity acting on the tangential diffusion term, we have performed core flow inversions from the geomagnetic secular variation. We acknowledge that interpreting core flow maps requires caution due to the uncertainties associated with the various assumptions necessary to perform the inversions, among which is the frozen-flux approximation (Holme 2007). Different flow models can explain the same observed secular variation, and it is likely that some flow features are erroneous in any inverted flow model. Studying the effects of each assumption is a complicated task. To highlight the influence of the frozen-flux approximation, we have compared inverted flows with and without magnetic diffusion, with all other inversion parameters unchanged. It is not guaranteed that our flow maps obtained with the diffusive model represent a significant improvement over those derived under different assumptions, but our consistent approach

of comparison between frozen-flux and diffusive flows using the same inversion scheme allows for inferring the possible impact of magnetic diffusion on core flow.

One weakness of our approach is that the correlation between radial and tangential diffusion at long wavelength is rather modest, even though statistically significant. It is not clear if the correlation degrades further for more Earth-like parameters. Parameterizing radial diffusion in terms of tangential diffusion will significantly improve the quality of the inverted core flow models if the correlation still holds at Earth-like conditions. If the correlation vanishes, there will be no improvement, but the comparison between diffusive and frozen-flux models can still serve to illustrate possible effects of diffusion on the inverted flow pattern and velocity and hence quantify the level of uncertainty of the frozen-flux model. We find that the inferred flow velocities become larger when diffusion is accounted for.

Another problem is that we need to extrapolate the values for the ratio of radial to tangential diffusion found in our numerical models over two orders of magnitude in the ratio Ra/Ra_c to obtain the value that we apply to the Earth's core. The resulting effective magnetic diffusivity is very large. The associated effective magnetic Reynolds number

$$Rm^* = \frac{UL}{\lambda^*} \tag{13}$$

is only of order one. This concurs with our finding that radial diffusion contributes on the order of 50 per cent to the secular variation at large wavelengths in our dynamo models, fairly independently of the values of the model parameters (Table 1). The small Rm^* values may seem worrisome since dynamo action requires a magnetic Reynolds number $Rm \gg 1$. However, our estimates of Rm^* and λ^* apply to radial diffusion at the top of the free stream and are not representative for the diffusion of the large-scale magnetic field in the dynamo in general. We found in the numerical dynamo models that radial diffusion becomes significantly weaker at depth, that is, the values of D and in particular of D_f are less at greater depth. The high effective diffusivity near the core–mantle boundary indicates that the large-scale magnetic field varies strongly in the radial direction in a magnetic boundary layer, whereas the variation with radius is smoother inside the dynamo.

In summary, we find that magnetic diffusion is likely to contribute significantly to the observed secular variation of the large-scale magnetic field at the core–mantle boundary. Taking its effect into account in models of the flow at the top of the core does not alter the pattern dramatically but leads to higher flow velocities and to important differences in flow structure in some regions.

ACKNOWLEDGMENTS

Numerical calculations were performed at the Service de Calcul Parallelle, IPGP. H.A. was supported by a grant from the IntraEuropean MarieCurie Action. H.A. thanks the Max-Planck Institute at Katlenburg-Lindau for their support and hospitality while initiating and finalizing this project. We thank Richard Holme and Coerte Voorhies for their useful suggestions and two anonymous reviewers for their insightful reviews. This is IPGP contribution 2408.

REFERENCES

Amit, H. & Olson, P., 2004. Helical core flow from geomagnetic secular variation, *Phys. Earth planet. Inter.,* **147,** 1–25.

Amit, H. & Olson, P., 2006. Time-average and time-dependent parts of core flow, *Phys. Earth planet. Inter.,* **155,** 120–139.

Amit, H., Olson, P. & Christensen, U., 2007. Tests of core flow imaging methods with numerical dynamos, *Geophys. J. Int.,* **168,** 27–39.

Amit, H., Aubert, J., Hulot, G. & Olson, P., 2008. A simple model for mantle-driven flow at the top of Earth's core, *Earth Planets Space,* **60,** 845–854.

Aubert, J., Amit, H., Hulot, G. & Olson, P., 2008. Thermo-chemical flows couple Earth's inner core growth to mantle heterogeneity, *Nature,* **454,** 758–761.

Bloxham, J., 1986. The expulsion of magnetic flux from the Earth's core, *Geophys. J. R. astr. Soc.,* **87,** 669–678.

Bloxham, J., 1989. Simple models of fluid flow at the core surface derived from geomagentic field models, *Geophys. J. Int.,* **99,** 173–182.

Bloxham, J. & Jackson, A., 1991. Fluid flow near the surface of the Earth's outer core, *Rev. Geophys.,* **29,** 97–120.

Braginsky, S. & LeMouël, J.-L., 1993. Two-scale model of a geomagnetic field variation, *Geophys. J. Int.,* **112,** 147–158.

Busse, F., 1975. A model of the geodynamo, *Geophys. J. R. astr. Soc.,* **42,** 437–459.

Christensen, U. & Aubert, J., 2006. Scaling properties of convection-driven dynamos in rotating spherical shells and application to planetary magnetic fields, *Geophys. J. Int.,* **166,** 97–114.

Christensen, U. & Olson, P., 2003. Secular variation in numerical geodynamo models with lateral variations of boundary heat flow, *Phys. Earth planet. Inter.,* **138,** 39–54.

Christensen, U. & Tilgner, A., 2004. Power requirement of the geodynamo from ohmic losses in numerical and laboratory dynamos, *Nature,* **439,** 169–171.

Christensen, U., Olson, P. & Glatzmaier, G., 1998. A dynamo model interpretation of geomagnetic field structures, *Geophys. Res. Lett.,* **25,** 1565–1568.

Chulliat, A. & Hulot, G., 2000. Local computation of the geostrophic pressure at the top of the core, *Phys. Earth planet. Inter.,* **117,** 309–328.

Eymin, C. & Hulot, G., 2005. On surface core flows inferred from satellite magnetic data, *Phys. Earth planet. Inter.,* **152,** 200–220.

Gubbins, D., 1987. Mechanism for geomagnetic polarity reversals, *Nature,* **326,** 167–169.

Gubbins, D., 1996. A formalism for the inversion of geomagnetic data for core motions with diffusion, *Phys. Earth planet. Inter.,* **98,** 193–206.

Gubbins, D. & Bloxham, J., 1987. Morphology of the geomagnetic field and implications for the geodynamo, *Nature,* **325,** 509–511.

Gubbins, D. & Gibbons, S., 2004. Low pacific secular variation, in *Timescales of the paleomagneteic field,* Geophysical monograph series, Vol. 145, eds Channell, J., Kent, D., Lowrie, W. & Meert, J., Washington, DC.

Gubbins, D. & Kelly, P., 1996. A difficulty with using the frozen flux hypothesis to find steady core motions, *Geophys. Res. Lett.,* **23,** 1825–1828.

Gubbins, D., Barber, C., Gibbons, S. & Love, J., 2000. Kinematic dynamo action in a sphere, I: Effects of differential rotation and meridional circulation on solutions with axial dipole symmetry, *Proc. R. Soc. Lond. A,* **456,** 1333–1353.

Holme, R., 2007. Large-scale flow in the core, in *Treatise on Geophysics,* Vol. 8, ed. Olson, P., Elsevier Science, London, 2007.

Holme, R. & Olsen, N., 2006. Core surface flow modelling from high-resolution secular variation, *Geophys. J. Int.,* **166,** 518–528.

Holme, R. & Whaler, K., 2001. Steady core flow in an azimuthally drifting reference frame, *Geophys. J. Int.,* **145,** 560–595.

Hulot, G., Eymin, C., Langlais, B., Mandea, M. & Olsen, N., 2002. Small-scale structure of the geodynamo inferred from Oersted and Magsat satellite data, *Nature,* **416,** 620–623.

Jackson, A., 1997. Time-dependency of tangentially geostrophic core surface motions, *Phys. Earth planet. Inter.,* **103,** 293–311.

Jackson, A., Bloxham, J. & Gubbins, D., 1993. Time-dependent flow at the core surface and conservation of angular momentum in the coupled core-mantle system, in *Dynamics of Earth's Deep Interior and Earth Rotation,* IUGG Vol. 12, eds LeMouël, J.-L., Smylie, D. & Herring, T., Geophysical Monograph 72, AGU.

Jackson, A., Jonkers, A. & Walker, M., 2000. Four centuries of geomagnetic secular variation from historical records, *Phil. Trans. R. Soc. Lond. A,* **358,** 957–990.

Kutzner, C. & Christensen, U., 2002. From stable dipolar towards reversing numerical dynamos, *Phys. Earth planet. Inter.,* **131,** 29–45.

Love, J., 1999. A critique of frozen-flux inverse modelling of a nearly steady geodynamo, *Geophys. J. Int.,* **138,** 353–365.

Masters, G., Laske, G., Bolton, H. & Dziewonski, A., 2000. The relative behavior of shear velocity, bulk sound velocity, and compressional velocity in the mantle: implications for chemical and thermal structure, in *Earth's deep interior,* **Vol. 117,** eds Karato, S., Forte, A., Liebermann, R., Masters, G. & Stixrude, L., AGU monograph, Washington, DC.

Olson, P. & Amit, H., 2006. Changes in earth's dipole, *Naturwissenschaften,* **93,** 519–542.

Olson, P. & Christensen, U., 2002. The time averaged magnetic field in numerical dynamos with nonuniform boundary heat flow, *Geophys. J. Int.,* **151,** 809–823.

Olson, P., Christensen, U. & Glatzmaier, G., 1999. Numerical modeling of the geodynamo: mechanisms of field generation and equilibration, *J. geophys. Res.,* **104,** 10 383–10 404.

Olson, P., Sumita, I. & Aurnou, J., 2002. Diffusive magnetic images of upwelling patterns in the core, *J. geophys. Res.,* **107,** doi:10.1029/2001jb000384.

Pais, M.A. & Jault, D., 2008. Quasi-geostrophic flows responsible for the secular variation of the Earth's magnetic field, *Geophys. J. Int.,* **73,** 421–443.

Poirier, J.-P., 2000. *Introduction to the Physics of the Earth's Interior,* Cambridge University Press, Cambridge, UK.

Press, W., Flannery, B., Teukolsky, S. & Vetterling, W., 1989. *Numerical Recipes (FORTRAN version),* Cambridge University Press, Cambridge, UK.

Rau, S., Christensen, U., Jackson, A. & Wicht, J., 2000. Core flow inversion tested with numerical dynamo models, *Geophys. J. Int.,* **141,** 485–497.

Roberts, P. & Scott, S., 1965. On analysis of the secular variation, 1, A hydromagnetic constraint: theory, *J. Geomagn. Geoelectr.,* **17,** 137–151.

Secco, R. & Schloessin, H., 1989. The electrical resistivity of solid and liquid Fe at pressures up to 7 GPa, *J. geophys. Res.,* **94,** 5887–5894.

Stacey, F. & Loper, D., 2007. A revised estimate of the conductivity of iron alloy at high pressure and implications for the core energy balance, *Phys. Earth planet. Inter.,* **161,** 13–18.

Voorhies, C., 1993. Geomagnetic estimates of steady surficial core flow and flux diffusion: unexpected geodynamo experiments, in *Dynamics of Earth's Deep Interior and Earth Rotation,* IUGG Vol. 12, eds LeMouël, J.-L., Smylie, D. & Herring, T., Geophysical Monograph 72, AGU.

Wicht, J., 2002. Inner-core conductivity in numerical dynamo simulations, *Phys. Earth planet. Inter.,* **132,** 281–302.